Strain Hardening Behavior of Ultrafine- Grained Cu by Analyzing the Tensile Stress-Strain Curve**

By *Chongxiang Huang, Shiding Wu, Shouxin Li* and *Zhefeng Zhang**

Ultrafine-grained (UFG) metals and alloys with grain sizes in a range of typically 100 nm ~ 1 μm exhibit high strength in accord with the well-known Hall-Petch relationship. Experimentally, when these new materials supplied high strength, their ductility, particularly uniform plastic strain in tension, was undesirably lower than that of their normally coarse-grained (CG) counterparts.[1–4] In recent years, many attempts have been made to develop methods for improving the ductility of UFG materials and several exciting results were obtained.[4–8] Ma and Wang summarized eight strategies to achieve coexisting high strength and high ductility at room temperature (RT) by tailoring the microstructures of UFG materials, such as introducing nano-precipitates in UFG matrix, using transformation-induced plasticity (TRIP) and twinning-induced plasticity (TWIP) etc.[9,10] Of these strategies, the most important issue was to increase strain hardening ability, which was essential for good uniform plastic strain because it could help delay localized deformation (necking instability) under tensile stress. Recently, Dalla Torre and the co-authors studied the strain hardening behavior of UFG Cu in compression, and indicated that UFG Cu showed hardening Stage III, IV and V, which was similar to those shown for metals deformed in other processes capable of high strain, such as torsion.[11,12] Under tensile stress, though most UFG metals produced by severe plastic deformation (SPD) were susceptible to necking instability, they did show some uniform plastic strain.[3–5,8,12–15] However, in most cases documented literature focused on the early necking of these metals.[2–5,12–17] It was inadequately understood how the uniform plastic strain of UFG metals advanced with increasing tensile stress. Therefore, it is of interest and necessary to study the strain hardening of UFG metals under uniaxial tensile stress, which is helpful for the understanding of the deformation mechanisms of these metals.

Strain hardening is commonly defined as the increase of flow stress with increasing plastic strain. Therefore, the analysis of stress-strain curves is very important for revealing the hardening behavior of materials. In general, there are three empirical fitting equations to illustrate the tensile stress-strain curves and the corresponding mathematical analyses based on these equations are used: the Hollomon analysis,[18] the Crussard-Jaoul (C-J) analysis based on the Ludwik equation,[19–21] and the modified C-J analysis based on the Swift equation.[22,23] Of the three analyses, it has been indicated that the modified C-J analysis is more sensitive to microstructures than the other two and able to distinguish the different stage of strain hardening of Al, Cu and steels with different microstructures.[23–25] For instance, Reed-Hill et al. successfully used the modified C-J analysis for identifying hardening Stage I, II and III of CG Cu.[23] In this work, the modified C-J analysis was also used to assess the tensile stress-strain curves of UFG Cu, in order to reveal its strain hardening behavior under uniaxial tensile stress.

The typical TEM microstructure of UFG Cu produced by ECAP for 8 passes is shown in Figure 1(a). It can be seen that the microstructure is characterized by submicro-sized grains with elongated shape. After 16 passes, the grains are not refined much more, but the grain shape becomes more equiaxed, as shown in Figure 1(b). At the same time, there are more sharp boundaries often with thickness fringes (indicated by white arrows in Figure 1(b)), which are considered to be high-angle grain boundaries (HAGBs).[26] Besides, a decrease of dislocation density within grains was also observed with increasing passes up to 16.[13,27] These microstructural characteristics imply that dynamic recovery has occurred during processing to many passes. Figure 1(c) shows the microstructure of Cu single crystal (SC) after ECAP deformation for one pass. It is seen that very small dislocation cells with sizes of 150 ~ 400 nm are distributed in a lamellar microstructure, which is very similar to that deformed by cold rolling. The microstructure of CG Cu deformed by ECAP for one pass is as similar as that of Figure 1(c).

[*] X. Huang, Prof. Z. F. Zhang
Shenyang National Laboratory for Materials Science
Institute of Metal Research
Chinese Academy of Sciences
Shenyang 110016, China
E-mail: chxhuang@imr.ac.cn, zhfzhang@imr.ac.cn

Prof. S. D. Wu, Prof. S. X. Li
Shenyang National Laboratory for Materials Science
Institute of Metal Research
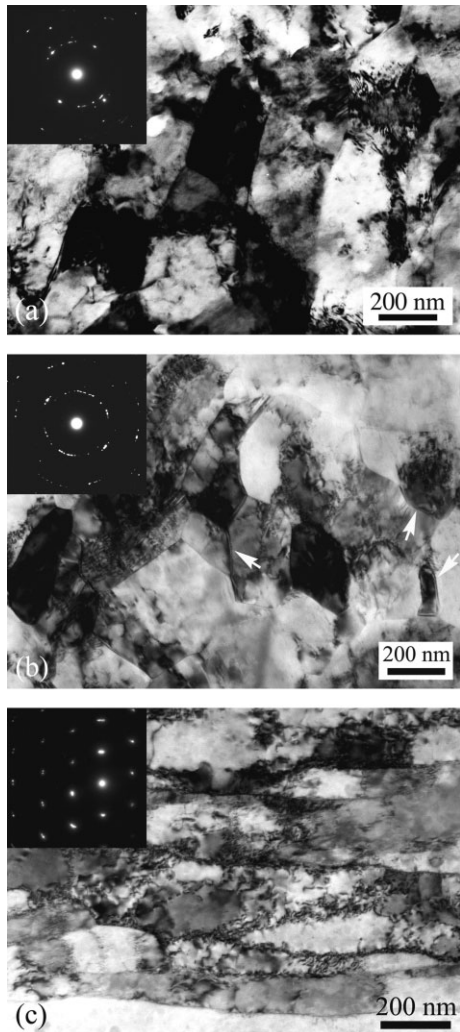Chinese Academy of Sciences
Shenyang 110016, China

Fig. 1. TEM micrographs of ECAP processed Cu: (a) UFG Cu, 8 passes, (b) UFG Cu, 16 passes, (c) single crystal, 1 pass. The bright arrows in (b) indicate the presence of GB fringes.

To further illustrate the characteristics of UFG microstructures, EBSD measurements were performed. Figure 2 presents the EBSD maps and corresponding GB misorientation distributions of UFG samples. It is seen that though the mean grain size (from EBSD) has been reduced to 367 nm for the 8 passed sample processed for, the microstructure is still inhomogeneous. There are several areas with sizes larger than 1 μm within which low-angle grain boundaries (LAGBs) are prevalent, as shown in Figure 2(a) (marked by "A" and "B"). The aspect ratio of grains is about 1.57. Figure 2(b) shows that most of GBs are LAGBs. The volume fraction of HAGBs (> 15 °) is only about 43%. By increasing passes up to 16, the grains are more equiaxed and homogeneous (see Fig. 2(c)), as reflected by the decreased aspect ratio of 1.17. The mean grain size is 334 nm. Figure 2(d) is the distribution of GB misorientation for the 16 pass sample. The volume fraction of HAGBs is increased up to ~ 74%, similar to previous measurements (~ 70%) by EBSD studies on Cu sample processed by ECAP for 14–20 passes.[12,28,29]

The tensile engineering stress-strain curves (converted from the load-displacement curves) of UFG Cu processed by ECAP for 8 and 16 passes are shown in Figure 3(a), Curves A and B. For comparison, the tensile curves of CG and SC Cu (Curves C and D, respectively) processed by ECAP for one pass (denoted as ECAP-1 samples) are also presented. It is seen that all of ECAP processed samples are sensitive to plastic instability and show little uniform plastic deformation, though their strengths are very high. In order to identify the yield strength (0.2% proof stress, $\sigma_{0.2}$) and the ultimate tensile strength (maximum stress, σ_b) accurately, the strain measured by extensometer is used to plot against stress, as shown in Figure 3(b). It can be seen obviously that the ECAP-1 samples show almost equal values of $\sigma_{0.2}$ and σ_b. The ratios of $\sigma_{0.2}/\sigma_b$ (see Tab. 1) are very close to 1, suggesting that they have almost lost the capability of strain hardening. By contrast, the UFG samples show some strain hardening, as identified by both the stress-strain curves and the ratios of $\sigma_{0.2}/\sigma_b$. Figure 3(c) presents the true stress-strain curves converted from the curves in Figure 3(b) by using the standard formula, showing clearly the differences of strain hardening of Cu with different microstructures.

To fit the tensile stress-strain curve (in the range of uniform plastic strain), the modified C-J analysis assumes that the stress-strain relationship follows the Swift equation:[22]

$$\varepsilon = \varepsilon_0 + c\sigma^m \qquad (1)$$

where ε and σ are the true stress and strain, respectively, ε_0 is the initial true strain, m is the strain hardening exponent, and c is the material constant. The differentiation of the logarithmic form of Equation 1 with respect to ε leads to the modified C-J analysis:[23]

$$\ln(d\sigma/d\varepsilon) = (1-m)\ln\sigma - \ln(cm) \qquad (2)$$

The slope of the $\ln(d\sigma/d\varepsilon)$ vs $\ln\sigma$ curve equals (1-m) and m can be obtained.

For CG Cu, the representative $\ln(d\sigma/d\varepsilon)$ vs $\ln\sigma$ curve is shown in Figure 4(a). Four stages of strain hardening processes and the transition strains can be easily identified. It should be pointed out that the Stage IV is usually observed at the end of strain hardening process in heavily cold-worked CG Cu after large strain.[30] In the present tensile test, the Stage IV is identified only in a plastic strain of ~ 3% prior to necking. The strain hardening exponents in Stages I, II, III given in Table 1 are consistent with those in literature.[24] For ECAP-1 samples (C and D in Fig. 4(b)), however, only one stage of strain hardening process was identified, showing higher values of m (70 ~ 80, Tab. 1) than that of the Stage IV, which should be the Stage V. It is reasonable to understand that, due to the extensive recovery of dislocations in the Stage V, a steady state flow stress appears, as shown in Figure 3(c) (Curves C and D).

As to UFG samples, it is interesting that two stages of strain hardening process are found, as shown in Figure 4(b) (Curves A and B). The values of m in these two stages are
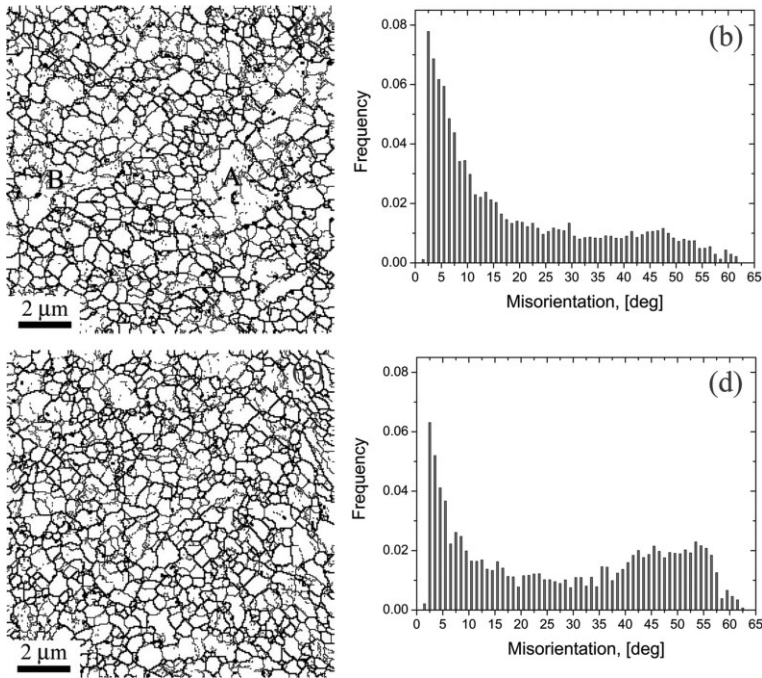
COMMUNICATIONS

Fig. 2. (a)-(b) EBSD map and misorientation measurement of UFG Cu, 8 passes, (c)-(d) EBSD map and misorientation measurement of UFG Cu, 16 passes. In (a) and (c), thick black lines mark boundaries with misorientation > 15 ° (HAGB), while thin gray lines market boundaries with misorientation < 15 ° (LAGB).

close to those of the Stage IV and the Stage V (see Tab. 1), respectively. Therefore, two different hardening processes could be identified for UFG Cu, which are analogous to the Stage IV and the Stage V. In *fcc* metals, the Stage IV is governed by athermal dislocation storage, whereas the Stage V is characterized by thermally activated recovery process, i.e., the equilibrium between generation and annihilation of dislocations.[30,31] In the case of UFG Cu, the mechanism of strain hardening in the first stage could stem from that there is a limited space in grains allowing certain storage of disloca-

Table 1 The processing state, ratio of $\sigma_{.\mu\sigma179.\mu\sigma163.\mu\sigma179.2}/\sigma_b$, uniform plastic strain ($\varepsilon_{plastic}$) and strain hardening exponent (m) obtained from the modified C-J analysis of different Cu samples.

	Samples	A	B	C	D	E
	States	8 passes	16 passes	1 pass	1 pass (SC)	CG
	Ratio of $\sigma_{0.2}/\sigma_b$	0.91 ± 0.01	0.86 ± 0.01	0.97 ± 0.01	0.99 ± 0.005	0.22 ± 0.1
	Uniform $\varepsilon_{plastic}$ (%)	1.24 ± 0.15	1.85 ± 0.14	0.62 ± 0.10	0.30 ± 0.10	40.2 ± 3.5
	m_I	–	–	–	–	1.4
	m_{II}	–	–	–	–	1.9
	m_{III}	–	–	–	–	3.1
m	m_{IV}	21.7	25.1	–	–	18.6
	m_V	76.4	83.1	82.6	70.9	–

tions. Accordingly, a fast increase of flow stress can be observed in the early stage of plastic strain, as shown in Figure 3(c) (in the range between the points marked with "*" and "│" in Curves A and B). However, it can not be expected that the strain hardening in this stage could sustain a large plastic strain because of the low efficiency of dislocation storage inside small grains at RT. After that, a stage of softening process resulted from dynamic recovery takes place and the flow stress increases very slowly until necking occurred (after the point marked with "│" in Curves A and B, Figure 3(c)). As a consequence, due to the limited capability of strain hardening in the first stage plus subsequent softening process in the second stage, UFG Cu exhibited only small uniform plastic strain at RT. This has been confirmed not only in UFG Cu, but also in many other UFG metals, such Ti and Ni.[15,16]

In accord with early investigations, the deformation process of UFG Cu is found to be complex and controlled by more than one mechanism. Intragranular dislocation strain and GB-mediated mechanism such as GB sliding and grain rotation have been confirmed experimentally.[8,13,32] The efficient dislocation slip and storage within grains can lead to a high strain hardening rate at low temperature.[8–13,32] As estimated by Valiev et al., the dislocation density in UFG Cu could be increased from 5×10^{14} to 10^{15} m^{-2} in the early stage of deformation.[32] This can explain the initial deformation stage with high stain hardening rate (Fig. 3(c)). With increasing the flow stress, dynamic recovery caused by annihilation of dislocations and GB-mediated deformation mechanism operated, resulting in a low strain hardening rate (the second hardening stage in Fig. 3(c)).[11,32] This deformation process can be promoted especially when GBs are in no-equilibrium state.[5,32]

To improve the strain hardening capability of UFG Cu, any effort should be based on the mechanism of strain hardening. In the first stage, the strain hardening capability could be improved by decreasing the initial dislocation density via several ways such as annealing,[14,15] pressing rod for many passes (more than 12 passes, as shown Fig. 1(c)),[5,13] and cyclic deformation.[33] However, the increase of uniform plastic strain at RT was still very limited because these methods did not intrinsically change the low efficiency of dislocation storage in small grains at RT, unless introducing micrometer-sized grains into the UFG matrix, such as a bi-model grain structure.[34] Another route to increasing the strain hardening capability was to suppress the rate of dynamic recovery of dislocations. The typical methods are to decrease the deformation temperature and/or to increase the tensile strain rate.[8,9] At
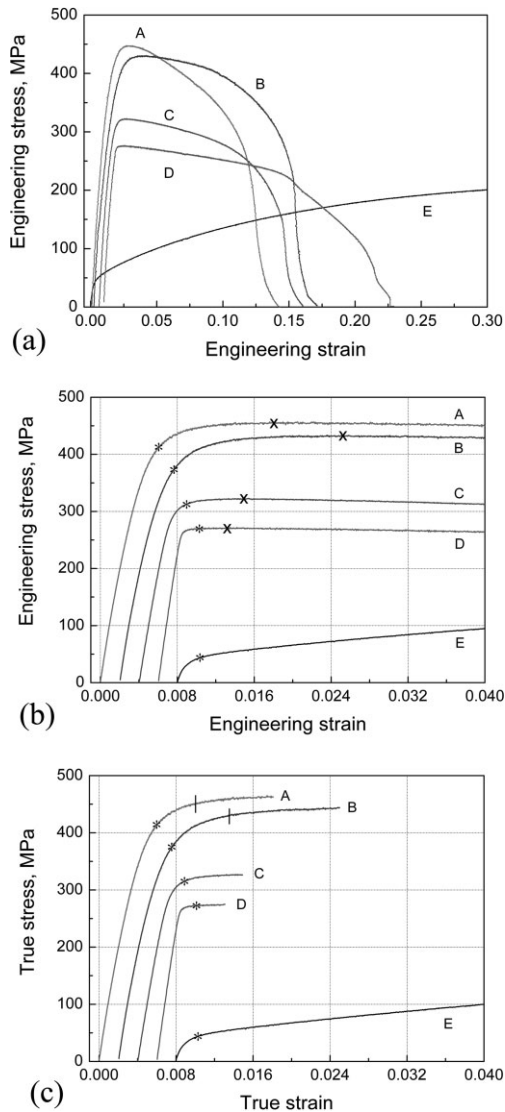
(a)

(b)

(c)

Fig. 3. (a) Engineering stress-strain curves of different Cu samples. The strain is trans-formed from the displacement of crosshead. Curve A, UFG Cu, 8 passes; Curve B, UFG Cu, 16 passes; Curve C, CG Cu, 1 pass; Curve D, SC Cu, 1 pass; Curve E, ini-tial CG Cu. (b) Engineering stress-strain curves used for the determination of strength and uniform plastic strain. The strain is measured by extensometer. The points of $\sigma_{0.2}$ and σ_b are marked with "*" and " × ", respectively. (c) True stress-strain curves con-verted from the curves in (b) using standard formula. The two stages of hardening process were detached by " | "

(a)

(b)

Fig. 4. ln (dσ/dε) vs. ln σ curves of (a) CG Cu and (b) ECAP processed Cu. More than one stages of strain hardening processes are identified in CG and UFG Cu. The transi-tion strains of different stages are also indicated.

low temperature, such as 77 K, the rate of dislocation recov-ery was very low, resulting in a higher dislocation storage, which inversely increased the strain hardening capability in the first stage.[8] Increasing the strain rate played the same function as decreasing temperature.[8,9] Consequently, a pro-nounced strain hardening was achieved, and both the uni-form plastic strain and the total elongation to failure were in-creased.[8,9]

In addition to the above methods, an alternative approach to achieve high ductility is to increase the strain rate harden-ing based on the Hart's instability criterion.[10] The enhanced strain rate sensitivity has been widely observed in UFG FCC metals.[5,8,11,35,36] By increasing strain rate sensitivity, GB-me-
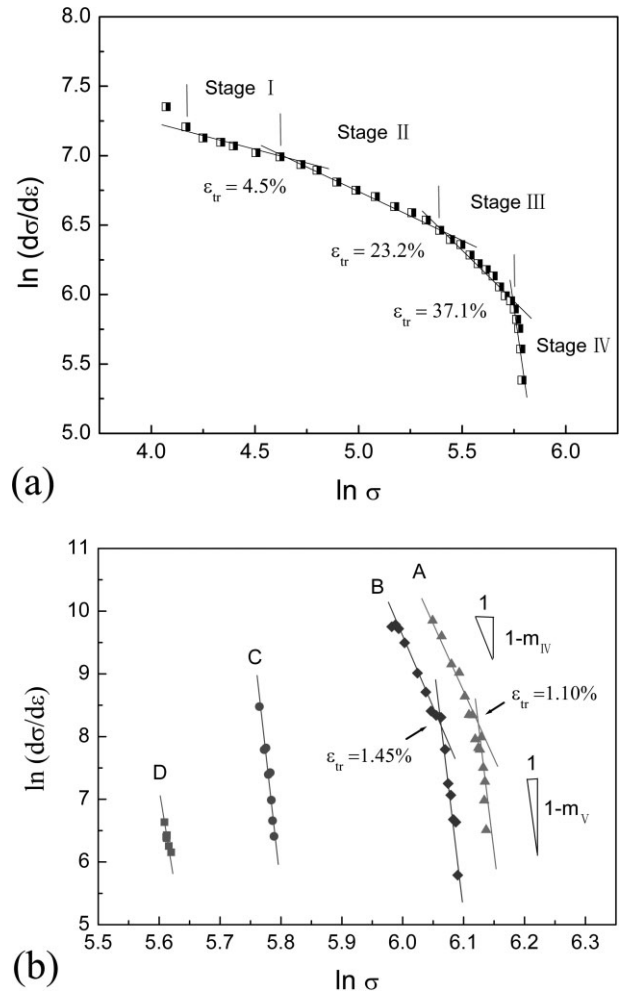
diated mechanisms are promoted for large uniform plastic deformation even without strain hardening, such as near-per-fect plastic deformation observed in UFG Cu at very low strain rate.[9,37] In this case, the key issue is to trigger GB-me-diated mechanisms, such as GB sliding and grain rotation. For most UFG metals produced by SPD, the GBs are usually in no-equilibrium state, with many dislocations that are not geometrically necessary for GB.[38] Therefore, it is proposed that by many SPD rounds, a microstructure comprising high fraction of HAGBs with no-equilibrium state can make an in-crease in uniform plastic strain (see example in Fig. 3).[4,5,39]

In summary, UFG Cu was found to experience two stages of strain hardening processes under uniaxial tensile stress, which was similar to the Stage IV and V of CG Cu after large plastic deformation. The storage of dislocations in small grains and dynamic recovery caused by annihilation of dislo-cations and GB-mediated processes were responsible for the different stages of strain hardening behavior. Improvement of strain hardening capability for UFG metals should be based on the mechanisms of strain hardening.

Experimental

In this study, two kinds of Cu rods (φ 10 mm × 85 mm) were used as the starting materials: commercial pure coarse-grained (CG) Cu (99.97%) with grain size of ~ 57 µm and Cu single crystal (SC) with [123] orientation (typically single-slip type) parallel to the longitudinal axis of its rod. The technique of equal channel angular pressing (ECAP) was used to process Cu rods. Both CG and SC samples were processed for one pass at RT (denoted as ECAP-1 samples). To produce UFG samples, the CG rods were processed up to 8 and 16 passes with route Bc (denoted as UFG samples). The detail procedures can be found in reference.[27]

The microstructures were examined by transmission electron microscope (TEM) and electron back-scatter diffraction (EBSD). The thin foils for TEM (JEM-2000FXII, operated at 200 kV) were cut from the as-processed rods parallel to its longitudinal axis (Y plane).[27] The thin foils were mechanical ground to ~ 50 µm using sand papers with different grades. Final thinning was conducted with twin-jet polishing in a solution of 25% phosphoric acid, 25% ethanol and 50% water. Specimens for EBSD measurements were cut from the as-processed rods perpendicular to its longitudinal axis (X plane). EBSD measurements were performed on a LEO-Supra 35 FEG-SEM with a step of 50 nm. The raw data were processed by HKL-Channel 5. Boundaries with misorientation angle larger that 3° were measured.

Tensile specimens were cut from as-processed rods with gauge size of 4 mm in width, 2 mm in thickness and 16 mm in length according to the standard relationship of $L_0=5.65 \times A^{1/2}$, where L_0 is the length and A is the cross-sectional area of the gauge part.[40] The quasistatic uniaxial tensile tests were performed at RT using an MTS 858 Mini Bionix machine with a crosshead speed of 0.48 mm/min (the equivalent strain rate, 5×10^{-4} s^{-1}). The data of the applied load and the displacement of crosshead and extensometer were collected by a PC computer.

[1] J. R. Weertman, D. Farkas, K. Hemker, H. Kung, M. Mayo, R. Mitra, H. Swygenhoven, *MRS Bull.* **1999**, *24*, 44.

[2] C. C. Koch, *J. Metastable Nanocryst. Mater.* **2003**, *18*, 9.

[3] E. Ma, *Scr. Mater.* **2003**, *49*, 663.

[4] R. Z. Valiev, T. G. Langdon, *Prog. Mater. Sci.* **2006**, *51*, 881.

[5] R. Z. Valiev, I. V. Alexandrov, Y. T. Zhu, T. C. Lowe, *J. Mater. Res.* **2002**, *17*, 5.

[6] Z. Horita, K. Ohashi, T. Fujita, K. Kaneko, T. G. Langdon, *Adv. Mater.* **2005**, *17*, 1599.

[7] Y. Ma, J. E. Jin, Y. K. Lee, *Scr. Mater.* **2005**, *52*, 1311.

[8] Y. M. Wang, E. Ma, *Appl. Phys. Lett.* **2003**, *83*, 3165.

[9] Y. M. Wang, E. Ma, *Acta Mater.* **2004**, *52*, 1699.

[10] E. Ma, *JOM* **2006**, *58*, 49.

[11] F. H. Dalla Torre, E. V. Pereloma, C. H. J. Davies, *Acta Mater.* **2006**, *54*, 1135.

[12] F. H. Dalla Torre, A. A. Gazder, E. V. Pereloma, C. H. J. Davies, *J. Mater. Sci.* **2007**, *42*, 9097.

[13] F. H. Dalla Torre, R. Lapovok, K. T. Remesh, P. F. Thomson, C. H. J. Davies, E. V. Pereloma, *Acta Mater.* **2004**, *52*, 481.

[14] Y. M. Wang, E. Ma, M. W. Chen, *Appl. Phys. Lett.* **2002**, *80*, 2395.

[15] D. Jia, Y. M. Wang, K. T. Remesh, E. Ma, Y. T. Zhu, R. Z. Valiev, *Appl. Phys. Lett.* **2001**, *79*, 611.

[16] C. D. Gu, J. S. Lian, Z. H. Jian, Q. Jiang, *Scr. Mater.* **2006**, *54*, 579.

[17] M. Dao, L. Lu, R. J. Asaro, J. T. M. De Hosson, E. Ma, *Acta Mater.* **2007**, *55*, 5041.

[18] J. H. Hollomon, *Trans. AIME* **1945**, *162*, 268.

[19] P. Ludwik, *Elemete der Technologischen Mechanik.* Berlin: Springer, **1909**. P. 32.

[20] C. Crussard, *Rev. Metall.* **1945**, *47*, 589.

[21] B. Jaoul, *J. Mech. Phys. Solid.* **1957**, *5*, 95.

[22] H. W. Swift, *J. Mech. Phys. Solid.* **1952**, *1*, 1.

[23] R. E. Reed-Hill, W. R. Gribb, S. N. Monteiro, *Metall. Trans.* **1973**, *4*, 2665.

[24] Y. Tomita, K. Okabayashi, *Metall. Trans. A* **1985**, *A16*, 865.

[25] Y. II. Son, Y. K. Lee, K. T. Park, C. S. Lee, D. H. Shin, *Acta Mater.* **2005**, *53*, 3125.

[26] W. H. Huang, C. Y. Yu, P. W. Kao, C. P. Chang, *Mater. Sci. Eng. A* **2004**, *366*, 221.

[27] C. X. Huang, K. Wang, S. D. Wu, Z. F. Zhang, G. Y. Li, S. X. Li, *Acta Mater.* **2006**, *54*, 655.

[28] O. V. Mishin, G. Gottstein, *Philos. Mag. A* **1998**, *78*, 373.

[29] A. Vinogradov, T. Suzuki, S. Hashimoto, K. Kitagawa, A. Kuznetsov, S. Dobatkin, *Mater. Sci. For.* **2006**, *503–504*, 971.

[30] M. Zehetbauer, V. Seumer, *Acta Metall. Mater.* **1993**, *2*, 577.

[31] P. Les, M. Zehetbauer, E. F. Rauch, I. Kopacz, *Scr. Mater.* **1999**, *41*, 523.

[32] R. Z. Valiev, E. Kozlov, Y. F. Ivanov, J. Lian, A. A. Nazarov, B. Baudelet, *Acta Mater.* **1994**, *42*, 2467.

[33] C. X. Huang, S. D. Wu, G. Y. Li, S. X. Li, *Mater. Sci. Eng. A* **2007**, in press.

[34] Y. M. Wang, M. W. Chen, F. H. Zhou, E. Ma, *Nature* **2002**, *419*, 912.

[35] Q. Wei, S. Chen, K. T. Ramesh, E. Ma, *Mater. Sci. Eng. A* **2004**, *381*, 71.

[36] Y. M. Wang, E. Ma, *Mater. Sci. Eng. A* **2004**, *375–377*, 46.

[37] Y. Champion, C. Langlois, S. Guerin-Mailly, J. L. Bonnentien, M. J. Hytch, *Sci.* **2003**, *300*, 310.

[38] R. Z. Valiev, R. K. Islamgaliev, I. V. Alexandrov, *Prog. Mater. Sci.* **2000**, *45*, 102.

[39] R. Z. Valiev, *Adv. Eng. Mater.* **2003**, *5*, 296.

[40] G. E. Dieter, *Mech. Metall.* New York: McGraw-Hill, **1986**, 293.